

See discussions, stats, and author profiles for this publication at: <https://www.researchgate.net/publication/51035641>

Aqueous Suspensions of Natural Swelling Clay Minerals. 1. Structure and Electrostatic Interactions

ARTICLE in LANGMUIR · MAY 2011

Impact Factor: 4.46 · DOI: 10.1021/la2001255 · Source: PubMed

CITATIONS

36

READS

95

9 AUTHORS, INCLUDING:



[Erwan Paineau](#)

French National Centre for Scientific Research

31 PUBLICATIONS 314 CITATIONS

[SEE PROFILE](#)



[Patrick Davidson](#)

Université Paris-Sud 11

176 PUBLICATIONS 4,517 CITATIONS

[SEE PROFILE](#)



[Pierre Emile Levitz](#)

Pierre and Marie Curie University - Paris 6

190 PUBLICATIONS 5,480 CITATIONS

[SEE PROFILE](#)



[Laurent J Michot](#)

French National Centre for Scientific Research

160 PUBLICATIONS 3,283 CITATIONS

[SEE PROFILE](#)

Aqueous Suspensions of Natural Swelling Clay Minerals. 1. Structure and Electrostatic Interactions

Erwan Paineau,^{*†} Isabelle Bihannic,[†] Christophe Baravian,[‡] Adrian-Marie Philippe,[‡] Patrick Davidson,[§] Pierre Levitz,^{||} Sérgio S. Funari,[†] Cyrille Rochas,[#] and Laurent J. Michot^{*†}

[†]Laboratoire Environnement et Minéralurgie, Nancy Université -CNRS, UMR 7569, BP40 54501 Vandœuvre Cedex, France

[‡]Laboratoire d'Energétique et de Mécanique Théorique et Appliquée, Nancy Université-CNRS, UMR 7563, 2 Avenue de la Forêt de Haye, BP160 54504 Vandœuvre Cedex, France

[§]Laboratoire de Physique des Solides UMR 8502, CNRS-Université Paris, Sud Bât 510, 91405 Orsay Cedex, France

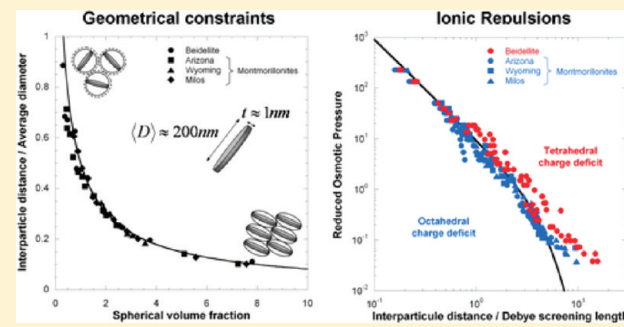
^{||}Laboratoire de Physique de la Matière Condensée UMR 7643, CNRS-Polytechnique Ecole Polytechnique, 91128 Palaiseau Cedex, France

[†]HASYLAB, NotkeStrasse 85, D-22603 Hamburg, Germany

[#]CERMAV-CNRS, BP 53, 38041 Grenoble Cedex 9, France

 Supporting Information

ABSTRACT: In this article, we present a general overview of the organization of colloidal charged clay particles in aqueous suspension by studying different natural samples with different structural charges and charge locations. Small-angle X-ray scattering experiments (SAXS) are first used to derive swelling laws that demonstrate the almost perfect exfoliation of clay sheets in suspension. Using a simple approach based on geometrical constraints, we show that these swelling laws can be fully modeled on the basis of morphological parameters only. The validity of this approach was further extended to other clay data from the literature, in particular, synthetic Laponite. For all of the investigated samples, experimental osmotic pressures can be properly described by a Poisson–Boltzmann approach for ionic strength up to 10^{-3} M, which reveals that these systems are dominated by repulsive electrostatic interactions. However, a detailed analysis of the Poisson–Boltzmann treatment shows differences in the repulsive potential strength that are not directly linked to the structural charge of the minerals but rather to the charge location in the structure for tetrahedrally charged clays (beidellite and nontronites) undergoing stronger electrostatic repulsions than octahedrally charged samples (montmorillonites, laponite). Only minerals subjected to the strongest electrostatic repulsions present a true isotropic to nematic phase transition in their phase diagrams. The influence of ionic repulsions on the local order of clay platelets was then analyzed through a detailed investigation of the structure factors of the various clay samples. It appears that stronger electrostatic repulsions improve the liquidlike positional local order.



1. INTRODUCTION

Swelling clays are ubiquitous minerals on the Earth's surface and subsurface and are largely used for industrial (drilling fluids, antisettling agents, ointments, cosmetics, etc.)^{1,2} and health applications.³ These high aspect ratio (20–1000) layered aluminosilicate compounds are typically formed from two tetrahedral layers (Si, Al, and Fe) encompassing an octahedral one (Al, Mg, and Fe). Isomorphic substitutions often occur in both layers, inducing a negative charge deficit compensated for by exchangeable cations located in the interlayer space. Most specific clay properties (i.e., swelling, thixotropy, and viscoelasticity) are linked to the valence and hydration properties of interlayer cations as well as to structural charge localization in the clay layer. The colloidal properties of swelling clay aqueous suspensions have

been intensively studied for more than a century since Freundlich first discovered their gelling behavior at a low volume fraction.⁴ Shortly afterwards, Langmuir reported a phase separation of suspensions of white California bentonite⁵ identified retrospectively as hectorite.⁶ Although phase separations, due to liquid-crystalline ordering, have been evidenced in various other mineral systems (e.g., oxides such as V_2O_5 ,^{7,8} $K_4Nb_6O_{17}$,^{9,10} and TiO_2 ,¹¹ hydroxides such as $Al(OH)_3$,^{12–15} and $NiOH$,^{16,17} oxyhydroxides such as $AlOOH$,^{18–20} and $\alpha\text{-FeOOH}$,^{21,22} layered double hydroxides such as Mg/Al LDH^{23,24}, and phosphates

Received: January 11, 2011

Revised: March 19, 2011

Published: April 08, 2011

Table 1. Chemical Formulae of the Studied Clay Samples^a

clay	origin	composition
SBId-1	Idaho	(Si _{7.27} Al _{0.73})(Al _{3.77} Fe ³⁺ _{0.11} Mg _{0.21}) O ₂₀ (OH) ₄ Na _{0.67}
SAz-1	Arizona	(Si _{7.95} Al _{0.05})(Al _{2.75} Fe ³⁺ _{0.17} Mg _{1.07}) O ₂₀ (OH) ₄ Na _{1.11}
SWy-2	Wyoming	(Si _{7.74} Al _{0.26})(Al _{3.06} Fe ³⁺ _{0.42} Fe ²⁺ _{0.03} Mg _{0.48}) O ₂₀ (OH) ₄ Na _{0.77}
Milos	Greece	(Si _{7.76} Al _{0.24})(Al ₃ Fe ³⁺ _{0.44} Fe ²⁺ _{0.02} Mg _{0.54}) O ₂₀ (OH) ₄ Na _{0.79}

^a Bold characters represent the main charge location.

such as H₃Sb₃P₂O₁₄²⁵), apart from Langmuir's work and until 2006,²⁶ studies on colloidal dispersions of natural or synthetic clay platelets have not allowed the observation of such a phase separation that appeared to be preempted by the sol–gel transition.^{27–31}

The structure of the gel and the mechanisms responsible for gelation have been debated since the 1930s with two conflicting views: (i) the so-called "house of cards" model based on the electrostatic attraction between the edges and faces of the platelets, leading to a tridimensional network^{32–35} and (ii) the stabilization of the gel structure by a repulsion between the interacting electrical double layers of the platelets.^{36–39} Making use of both models, Abend and Lagaly proposed a general phase diagram for sodium montmorillonites⁴⁰ showing a repulsive gel at low ionic strength (<10⁻³ M) and high volume fraction, whereas at higher ionic strength only attractive interactions were involved whatever the clay concentration. In the past decade, light, X-ray, and neutron scattering techniques performed on synthetic Laponite confirmed this general picture^{41–49} but favored the formation of a repulsive "Wigner" colloidal glass at low ionic strength.^{50–58} In the case of natural clay suspensions, experimental measurements^{31,59–64} and simulation works^{65–69} have pointed out the relevance of repulsive interactions in clay suspensions due to double-layer electrostatic forces.

Surprisingly, the effect of charge location on the phase behavior of clay suspensions has been little investigated, although it was shown that interactions between tetrahedrally substituted clay platelets differ significantly from those between octahedrally substituted particles.⁷⁰ This was confirmed by recent work that we carried out on size-selected suspensions of natural and perfectly exfoliated nontronite clays with a tetrahedral charge substitution, where we could see a clear isotropic to nematic phase transition at a volume fraction lower than the sol–gel transition.^{26,71,72} In contrast to the usual isotropic phase, the clay sheets in the nematic phase tend to align parallel to each other and therefore have long-range orientational order. A nontronite with a higher structural charge displays similar behavior.⁷³ Finally, we also recently reported a first-order isotropic/nematic transition in suspensions of natural disk-shaped beidellite, another tetrahedrally substituted clay closely related in shape to montmorillonites.⁷⁴

It then appears that charge location could be a key feature in the phase behavior of swelling clay minerals because the isotropic/nematic transition is masked by the gelation process for all octahedrally substituted clay minerals studied so far.⁷⁵ To understand these differences better, this article reports a detailed SAXS investigation of the structure of various size-selected clay platelet suspensions with different charge locations at various ionic

Table 2. CEC Values (meq/100g) Determined by the Cobalt Hexamine Exchange Procedure⁷⁹

size	SBId-1	SWy-2	SAz-1	Milos
S1	64.2	96.4	123.8	98.9
S2	83.3	96.6	124.8	97.4
S3	94.3	96.4	122.5	96.3
S4		nd	124.6	126.4

Table 3. Comparison of the Structural Charges (C·m⁻²) Obtained from the Chemical Formula (σ_{cation}) and from the CEC Values (σ_{CEC}) for Beidellite and Montmorillonites

size	SBId-1	SWy-2	SAz-1	Milos
σ_{cation}	-0.119	-0.137	-0.198	-0.141
σ_{CEC} S1	-0.114	-0.172	-0.220	-0.176
σ_{CEC} S2	-0.148	-0.172	-0.222	-0.173
σ_{CEC} S3	-0.168	-0.172	-0.218	-0.171
σ_{CEC} S4		nd	-0.222	-0.225

strengths. By collating the data thus obtained with osmotic pressure measurements, we then analyze in some depth the influence of both electrostatic interactions and excluded volume effects for various clay minerals including laponite.

2. MATERIALS AND METHODS

2.1. Sample Preparation. Four reference natural swelling clay minerals from the montmorillonites group⁷⁶ were chosen for this study. One beidellite (SBId-1, Idaho) and two montmorillonites (SAz-1, Arizona; SWy-2, Wyoming) were purchased from the Source Clays Minerals Repository of the Clay Mineral Society (Purdue University). The last montmorillonite from Milos, Greece was kindly provided by Iko Erbslöh (Germany). Because all of these samples are natural clays, isomorphous substitutions occur in both the tetrahedral (Si → Al, Fe) and octahedral layers (Al → Mg).⁷⁷ In the case of beidellite, the charge is mainly located in the tetrahedra whereas montmorillonites are mainly octahedrally charged. The chemical formulas of these four samples, deduced from chemical analyses,^{74,78} are summarized in Table 1.

Prior to use, natural clay samples were purified of accessory minerals such as quartz, feldspar, and oxyhydroxides and sodium exchanged. A size fractionation procedure was then applied by successive centrifugation, and four size fractions were obtained, referenced in the following study as S1 to S4 except for beidellite, which has only three size fractions. (Indeed, for beidellite, the residual supernatant obtained after the last centrifugation was almost devoid of clay particles.) For each size, the mineralogical purity was checked by X-ray diffraction and infrared spectroscopy, and the cationic exchange capacity (CEC) was determined by exchange with cobalt hexamine⁷⁹ (Table 2). The CEC for the smallest Wyoming (SWy-2) size fraction could not be determined because of the small concentration of particles in the residual suspension.

The value obtained for size 1 beidellite is somewhat low. This is due to the presence in this size fraction of small amounts of kaolinite (around 10%) after the purification process, as revealed by X-ray powder diffractograms. If one excludes this latter value, then it appears that the CEC values are fairly constant whatever the size fraction, except for the smallest size fraction of Milos montmorillonite. Then, by taking into account the unit cell dimensions of the basal surface (0.45 nm²), the structural charge can be calculated using the number of compensating cations or the CEC value. Table 3 summarizes the values obtained by both methods. Typical charges evolve between -0.1 and -0.2 C·m⁻².

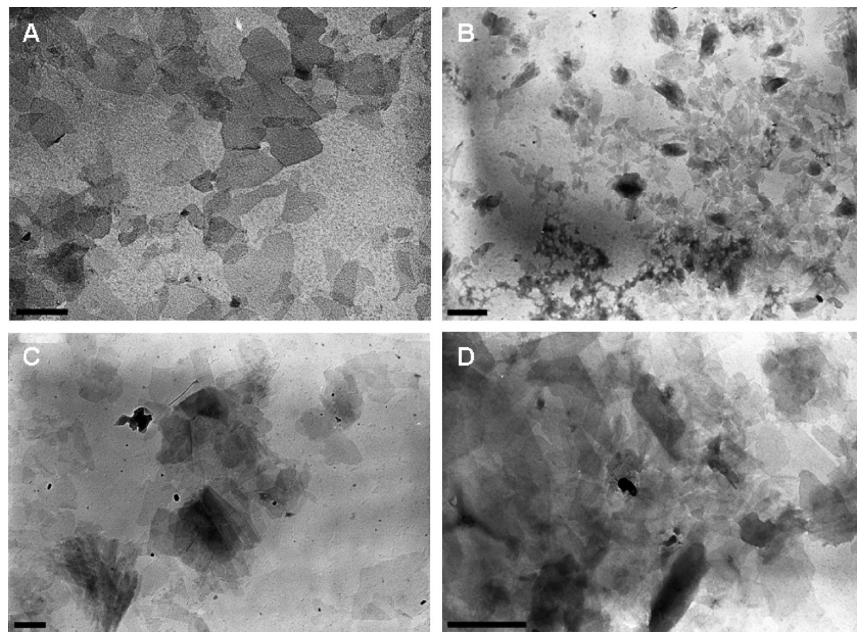


Figure 1. TEM micrographs of different size fractions of sodium smectites. (A) SBId-1 S3, (B) SAz-1 S2, (C) SWy-2 S2, and (D) Milos S2. The scale bar corresponds to 0.3 μm .

The charge density calculated from the CEC is still higher than those determined from the chemical formulae. Indeed, this method takes into account the charges induced by isomorphic substitutions as well as those resulting from broken bonds on the particle edges.

The morphological parameters of each size fraction were determined by transmission electron microscopy (TEM) using a CM12 Philips microscope operating at 80 kV. A drop of a dilute clay suspension ($\sim 20 \text{ mg/L}$) was deposited and air dried on a carbon-coated copper grid before observation. From the TEM micrographs, the average diameter $\langle D \rangle$ and its polydispersity σ_D , defined as the relative standard deviation,

$$\sigma_D = \frac{\sqrt{\langle D^2 \rangle - \langle D \rangle^2}}{\langle D \rangle} \quad (1)$$

were obtained from the analysis of around 150 particles.

Batches of suspensions were prepared from the stock suspension for each size at a fixed ionic strength (10^{-5} – 10^{-3} M) by osmotic stress⁸⁰ by using regenerated cellulose dialysis tubes (Visking, MWCO = 14 000 Da, Roth) and poly(ethylene glycol) solutions (PEG 20 000, Roth). The imposed pressures Π_{osm} were chosen to obtain suspensions covering the entire phase diagram, from the sol to the gel. All details of sample preparations have already been presented elsewhere.⁷⁴ As shown previously,⁷² more concentrated dispersions should provide a better accuracy for determining the value of the effective charge. Additional measurements beyond $\Pi_{\text{osm}} = 10 000 \text{ Pa}$ were then performed by filling membranes with 140 cm^3 of clay suspensions and placing them into 2000 cm^3 of PEG solutions. At the end of the experiment, the clay suspensions were recovered and their volume fractions were calculated to be

$$\phi = \frac{C_r}{\rho_{\text{vol}}} \quad (2)$$

with C_r being the “real” solid content accounting for the relative humidity according to the water adsorption isotherm of sodium saponite⁸¹ for tetrahedrally substituted clays and of sodium montmorillonite,⁸² and ρ_{vol} the specific mass of the clay particles, taken as 2.62 and 2.7 g cm^{-3} for beidellite and the montmorillonites, respectively.

2.2. Small Angle X-ray Scattering. Samples of clay suspensions were held in cylindrical glass capillaries (GLAS, Schönwalde bei Berlin, Germany) of 1 mm diameter that were both flame and wax sealed to prevent water evaporation. Small-angle X-ray scattering (SAXS) experiments were carried out on beamline A2 at HASYLAB (Hamburg, Germany) and on French CRG beamline D2AM at ESRF (Grenoble, France). Measurements at A2 were carried out at a fixed wavelength of 0.15 nm and a sample to detector distance of 2.48 m, and the scattering patterns were collected on a MarCCD whereas D2AM experiments used a wavelength of 0.11 nm, a sample to detector distance of 1.66 m, and a fiber-optic-coupled Roper Scientific CCD camera. The curves of scattering intensity versus scattering vector modulus q ($q = 4\pi \sin \theta / \lambda$, where 2θ is the scattering angle and λ is the wavelength) were deduced from the azimuthal angular integration $[0, 2\pi]$ of the SAXS patterns previously corrected for water and glass scattering.

3. RESULTS

3.1. Size Measurements. Geological history influences mineral crystallization, thus resulting in various morphological habits for natural clay particles, with all arising from a perfect hexagonal form.⁷⁷ Representative TEM micrographs of the four studied smectites are presented in Figure 1. SBId-1, SAz-1, SWy-2, and Milos swelling clays form thin platelets with subhexagonal shapes,⁷⁷ in agreement with previous TEM^{31,83} and AFM⁸⁴ observations. Because of this irregular shape, the mean diameter was taken as the longest chord within each particle, thus assuming as a first approximation a discoidal shape for the particles.

The deduced morphological parameters are presented in Table 4, except for the smallest size fractions of the Wyoming (SWy-2) and Arizona (SAz-1) clays, which are barely visible with the transmission electron microscope.

The polydispersity of the raw clay was typically around 60 for beidellite and 8–130 for montmorillonites. As expected, these values decrease with size fractionation but still remain relatively high.

Table 4. Morphological Parameters of the Different Size Fractions of Beidellite and Montmorillonite Clays^a

name	SBId-1				SAz-1				SWy-2				Milos			
size	S1	S2	S3	S1	S2	S3	S4	S1	S2	S3	S4	S1	S2	S3	S4	
average diameter (nm)	326	286	209	295	150	95	60	410	240	100	40	310	205	140	100	
polydispersity diameter (%)	47	45	38	90	42	19	nd	130	93	45	nd	80	41	17	8	

^a Italic values correspond to estimated number-averaged diameters.

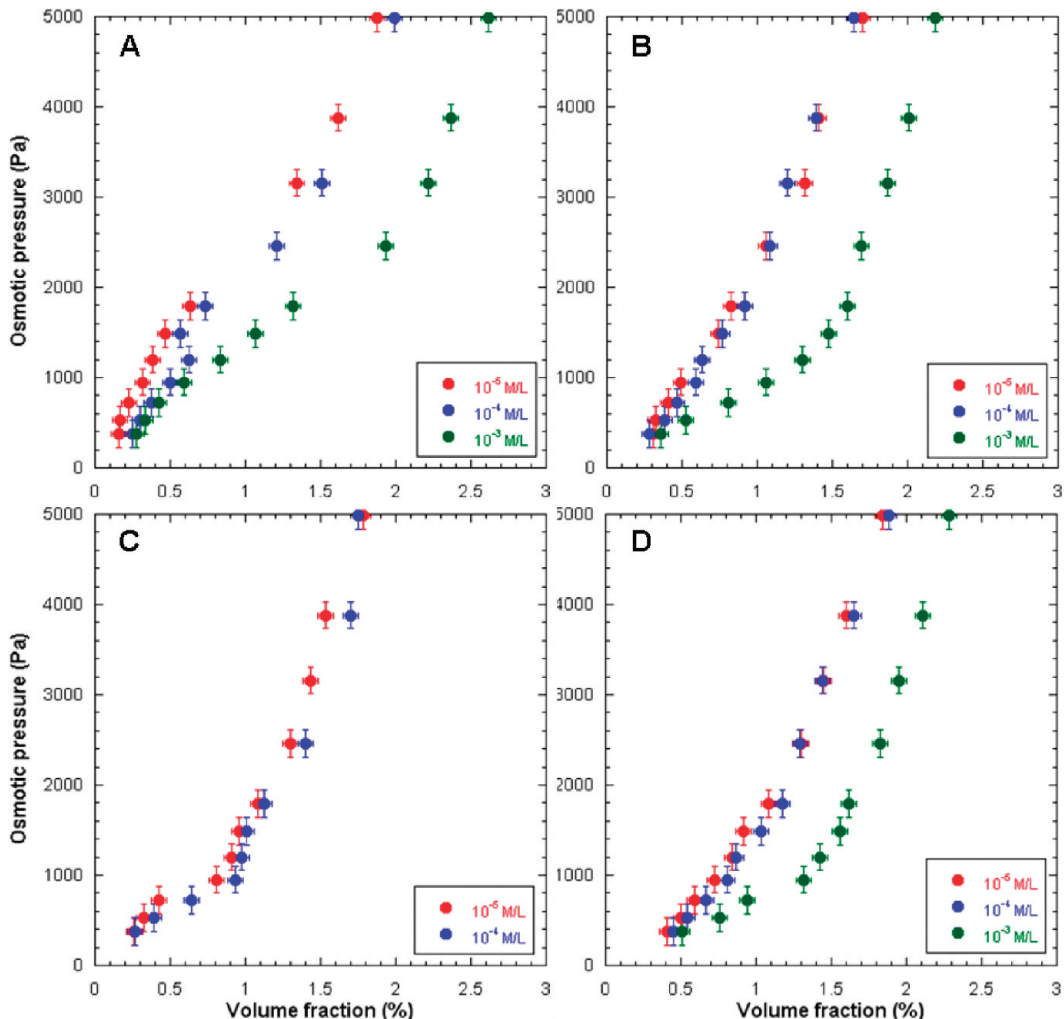


Figure 2. Osmotic pressure curves at various ionic strengths. (A) SBId-1 S3, (B) SAz-1 S2, (C) SWy-2 S2, and (D) Milos S2.

3.2. Osmotic Pressure Measurements. Figure 2 presents the osmotic pressure curves obtained by applying pressures of up to 5000 Pa to beidellite and montmorillonites of similar sizes at different ionic strengths. All curves display similar shapes, and in all cases, reducing the ionic strength leads to an increase in osmotic pressure, in agreement with the screening of the Debye length. However, some differences can be noticed. First, the osmotic pressure of beidellite is higher than those of montmorillonites at low volume fraction, whereas the opposite behavior is observed at high volume fraction. Second, the curves corresponding to Wyoming (SWy-2) montmorillonite are different, with a slight increase in the osmotic pressure between 500 and 1000 Pa that is not observed for any of the other samples. However, no clear pseudoplateau separating both liquid and gel phases has been reported.^{27,29,31}

3.3. SAXS Measurements. SAXS experiments were carried out to assess the structure of the clay suspensions throughout the whole phase diagrams. Whatever the clay used, in the dilute regime where the scattering is dominated by the particle form factor, the SAXS pattern is still isotropic and the scattering intensity follows a q^{-2} dependence of the scattering vector modulus, which confirms the bidimensional nature of isolated scattering objects.

Figure 3 displays SAXS patterns obtained for concentrated gel suspensions of beidellite and montmorillonites. With increasing volume fraction, 2D SAXS patterns are anisotropic as a result of elongational alignment upon capillary filling^{71,74} and marked diffuse peaks corresponding to the short-range positional order of the platelets are observed.

An estimate of the experimental average interparticle distance, \bar{D}_{exp} , can then be deduced from the position of the maximum in

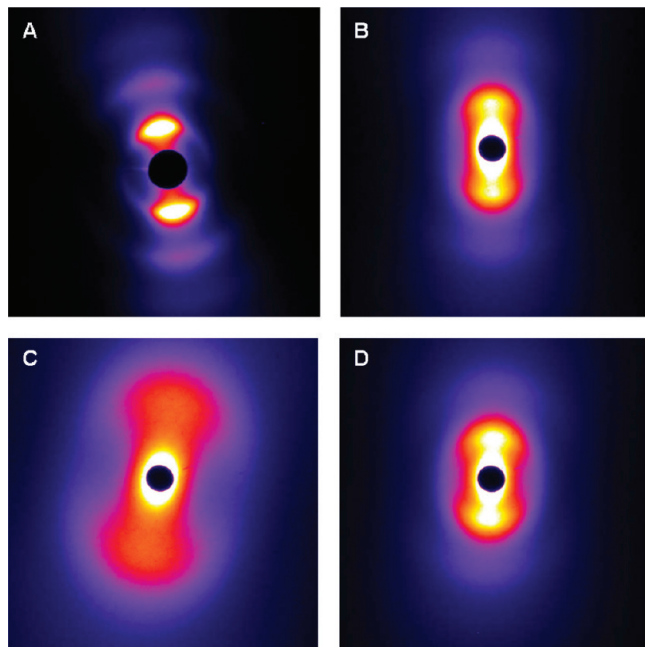


Figure 3. Two-dimensional SAXS patterns of clay gels at an ionic strength of 10^{-4} M. (A) SBId-1 S3, $\phi = 1.99\%$; (B) SAz-1 S2, $\phi = 1.64\%$; (C) SWy-2 S3, $\phi = 4.05\%$; and (D) Milos S2, $\phi = 1.88\%$.

the oscillations of the scattering intensity as

$$\bar{D}_{\text{exp}} \approx \frac{2\pi}{q_{\max}} \quad (3)$$

With this relation, swelling laws relating the interparticle distance to the volume fraction can be deduced. Figure 4 represents such swelling laws for various ionic strengths for beidellite and montmorillonites with an average diameter of 200 nm. Swelling laws obtained for other sizes are presented in the Supporting Information.

Whatever the clay type, size fraction, or ionic strength, the swelling laws are rather similar in shape and exhibit two distinct domains. At low volume fractions, the experimental average interparticle distances tend to scale as $\phi^{-1/3}$, which can be assigned to the 3D swelling of freely rotating objects. At higher volume fractions, a crossover occurs to a ϕ^{-1} unidimensional swelling regime related to the local lamellar order of the clay particles. Such an evolution has already been described for natural (SWy-1 montmorillonite^{59,60} and nontronites^{72,73}) or synthetic (Laponite⁴⁶) clay suspensions as well as for gibbsite particles.⁸⁵ In the ϕ^{-1} regime, the average thickness, t , of the individual platelets can be derived from the slope of the swelling law²⁵ by considering that

$$\bar{D}_{\text{exp}} = \frac{\langle t \rangle}{\phi} \quad (4)$$

The average values obtained for all samples are reported in Table 5.

In most cases, the obtained values are close to the thickness of a single clay sheet of around 0.7 nm, which suggests the perfect exfoliation of the clay sheets in such suspensions. This is not quite as true for the largest particles that exhibit thickness values of around 1 nm. This could be assigned to the presence in suspension of some doublets of particles, as already observed in

such suspensions.^{70,86} For simplicity, such size fractions will not be used in the following text even though they display similar behavior.

4. DISCUSSION

As shown recently,^{72,87} the distance between platelets can be well described using the expression

$$\bar{D}_{\text{th}} = \frac{\langle D \rangle}{\left(\frac{\phi_{\text{sph}}}{\phi_{\text{sph}}^*} \right)^{1/3} + \left(\frac{\phi_{\text{sph}}}{\phi_{\text{sph}}^*} \right)} \quad (5)$$

where \bar{D}_{th} is the calculated interparticle distance, $\langle D \rangle$ is the average diameter, ϕ_{sph} is a spherical volume fraction representing the fraction of the volume encompassing freely rotating particles and defined as $\phi_{\text{sph}} = 2/3\langle D \rangle/t\phi$ for disks, and $\phi_{\text{sph}}^* = 1$.^{72,87} Figure 5 confirms such a statement by displaying, for beidellite and for the three montmorillonite samples used in the present study, the evolution of the experimental interparticle distances rescaled by the average diameter of the clay platelets as a function of the volume fraction and comparing it with the results of eq 5 (solid line).

This approach can in principle be extended to any clay suspension.⁸⁷ To test such an assertion, Figure 6 displays the application of eq 5 to small-angle neutron scattering data obtained by Ramsay and Lindner on dispersions of Wyoming (SWy-1) sodium montmorillonite⁶⁰ ($\langle D \rangle \approx 250$ nm, $t \approx 0.65$ nm) and by Martin and co-workers on concentrated suspensions of Laponite XLG ($\langle D \rangle \approx 30$ nm and $t \approx 1.35$ nm) in the presence and absence of an added polyphosphate ($\text{Na}_4\text{P}_2\text{O}_7$).⁴⁶

Good agreement is obtained by simply using the morphological parameters determined by these authors from conventional techniques (TEM and scattering experiments).

Because we know the average interparticle distance for each point on the phase diagram, it is worthwhile to assess the role of electrostatic interactions by comparing the osmotic pressures obtained from experimental measurements (Figure 2) and theoretical calculations. As shown by Michot et al.,⁷² the Poisson–Boltzmann (PB) equation can be solved analytically for the case of two strongly charged parallel infinite plates ($\sigma = -0.11 \text{ C m}^{-2}$) and a half-separation distance (H) between plates of much greater than ~ 0.3 nm (appendix of ref 72) in a symmetrical 1:1 electrolyte solution. By plotting, for each sample, the evolution of the reduced osmotic pressure as a function of the ratio of the interparticle distance to the Debye length, further information about the repulsion between clay platelets can be derived (Figure 7A).

According to this Figure, two subgroups of samples can be distinguished. Experimental points corresponding to beidellite are located at high osmotic pressure, whereas montmorillonites exhibit significantly lower values. The electrostatic repulsions between platelets then decrease in the order beidellite \geq Milos, Wyoming (SWy-2), and Arizona (SAz-1) montmorillonites. To emphasize even more the importance of the type of clay used, we have added to Figure 7 Laponite data points that represent osmotic pressure measurements performed by Mourchid and co-workers^{27,29} on Laponite RD and the average interparticle distances calculated from the effective geometrical approach described above (eq 5). In the framework of such assumptions, the repulsive interactions of Laponite are clearly less intense.

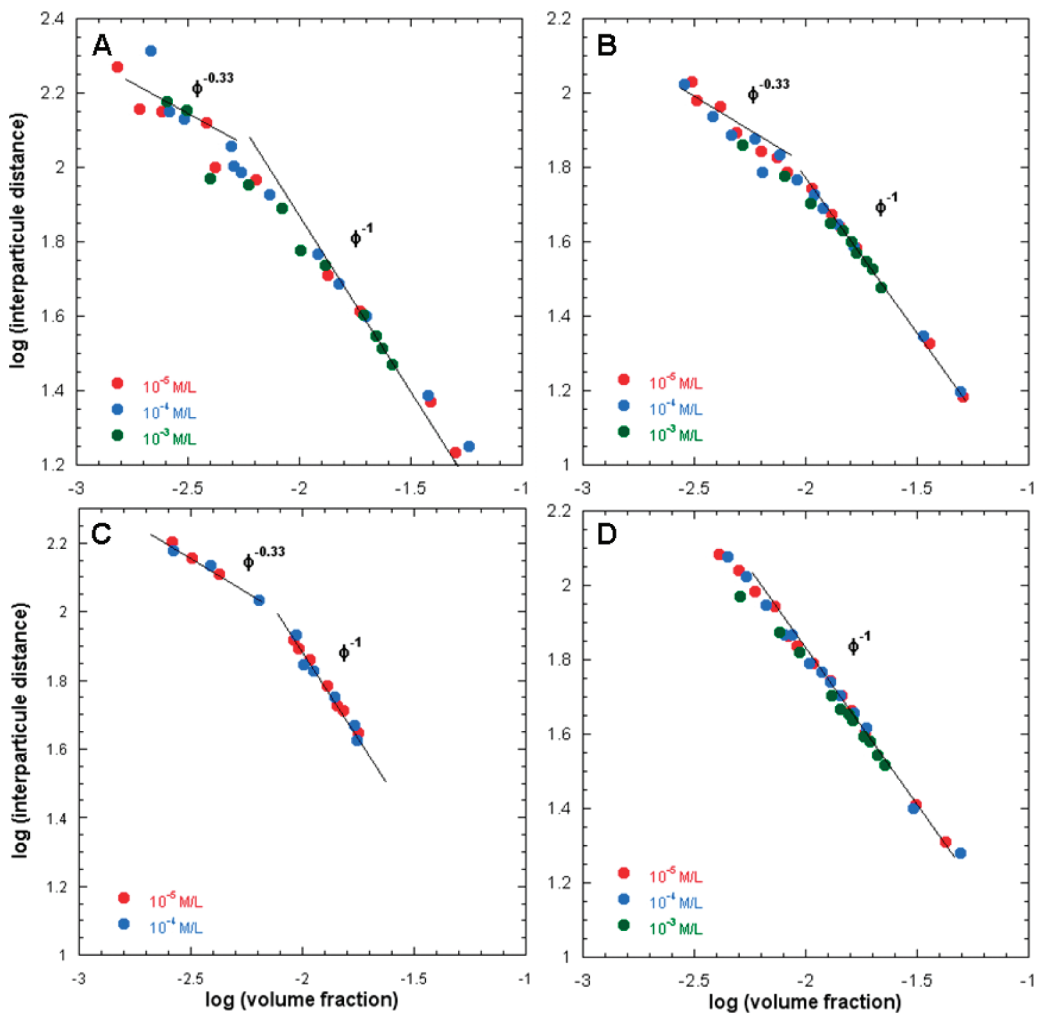


Figure 4. Variations in the swelling laws at various ionic strengths for smectite suspensions with an average diameter of 200 nm. (A) SBId-1 S3, (B) SAz-1 S2, (C) SWy-2 S2, and (D) Milos S2. Distances are reported in nanometers.

Table 5. Obtained Values of the Average Thickness^a Derived from Swelling Laws by Using Equation 4

name	SBId-1	SAz-1	SWy-2	Milos
S1	1.1	1	1	1.05
S2	0.85	0.7	0.8	0.75
S3	0.7	0.7	0.75	0.7
S4		0.65	0.65	0.7

^aIn nanometers.

It must be emphasized that the sequence thus determined experimentally is not related to the structural charge of the clay (Table 2) because Arizona (SAz-1) montmorillonite, with the highest structural charge, is one of the least repulsive samples. It seems, however, that tetrahedrally substituted clays are more repulsive than octahedrally substituted ones. To assess such an assumption, we have represented the experimental values of electrostatic repulsions as a function of charge location in the clay (Figure 7B). In the case of nontronites, another tetrahedrally substituted clay, the obtained values of electrostatic repulsions (not shown) are roughly intermediate between those of beidellite and montmorillonites. This discrepancy

should be due to the very anisometric shape of the nontronite laths. As expected, the electrostatic repulsive interactions of beidellite differ significantly from those between montmorillonites. This is in agreement with the observations of Lubetkin.⁷⁰ This nontrivial⁸⁸ behavior also correlates with the observation, for nontronites^{26,71–73} and beidellite⁷⁴ suspensions, of a clear I/N phase transition in addition to the sol–gel transition whereas only the sol–gel transition was observed for montmorillonites.^{27–31} Further theoretical work clearly needs to be performed to fully assess and characterize the influence of charge location.

The use of the PB equation has demonstrated that the repulsion strength depends on the type of clay, and this should affect the local order of the platelets. Indirect evidence of such an influence is shown in Figure 3. At equivalent average size and spherical volume fraction, the obtained SAXS patterns are distinctly different for clay minerals that display similar swelling laws. Beidellite displays markedly diffuse scattering peaks whereas the scattering peaks of the montmorillonites are systematically much broader. In the following text, we will focus on disk-shaped clay particles only, a simpler situation than that of the lath-shaped nontronites, even though similar behaviors are observed in the case of nontronite NAu-2.⁷² Information about the positional

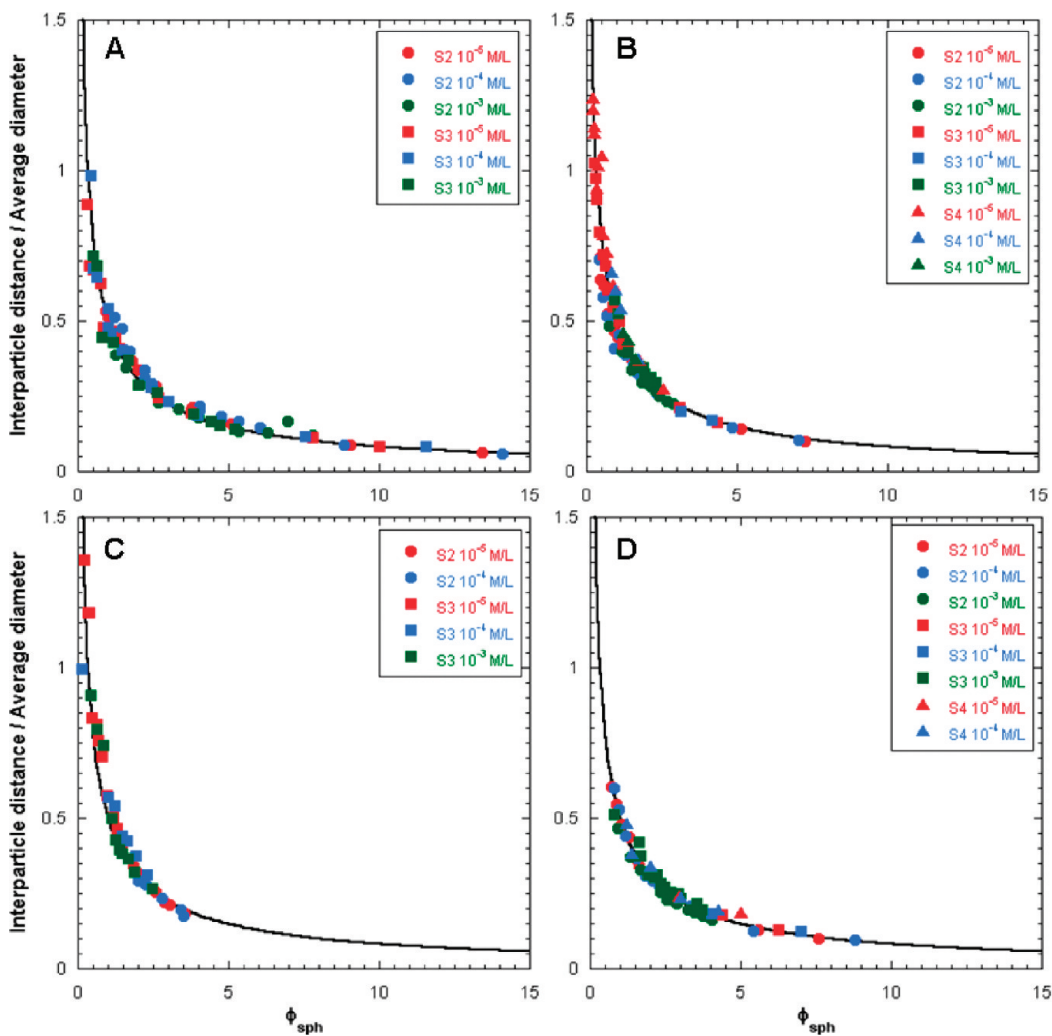


Figure 5. Evolution of the ratio of interparticle distance/average diameter as a function of the volume fraction of equivalent spheres. (A) SBId-1, (B) SAz-1, (C) SWy-2, and (D) Milos. The solid line corresponds to eq 5 with $\phi_{\text{sph}}^* = 1$.

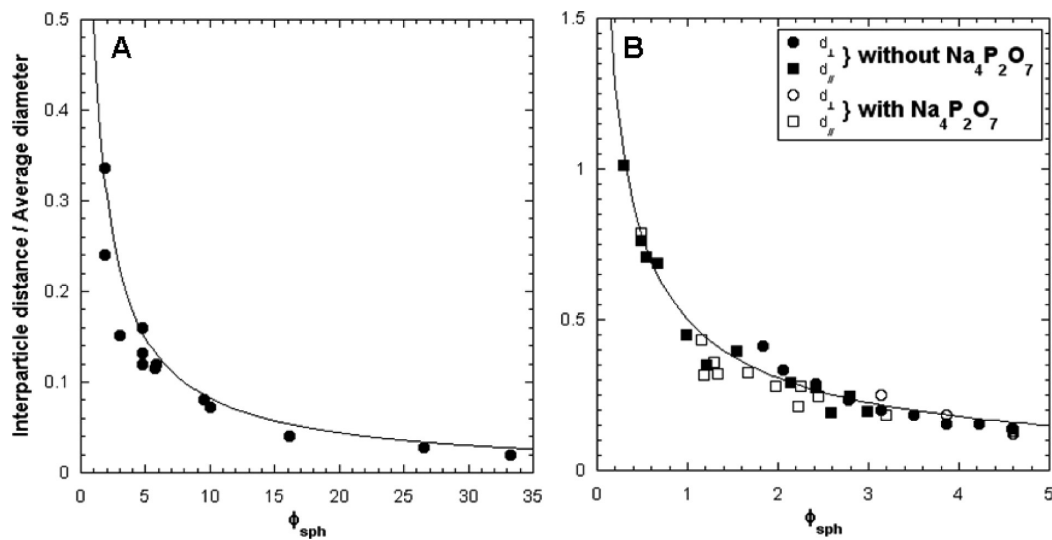


Figure 6. (A) Dispersions of SWy-1.⁶⁰ (B) Longitudinal (d_{\perp}) and transverse (d_{\parallel}) slices of highly concentrated Laponite suspensions.⁴⁶ Closed symbols represent dispersions without phosphates, and open symbols represent dispersions with phosphates. In all cases, the solid line correspond to eq 5 with $\phi_{\text{sph}}^* = 1$.

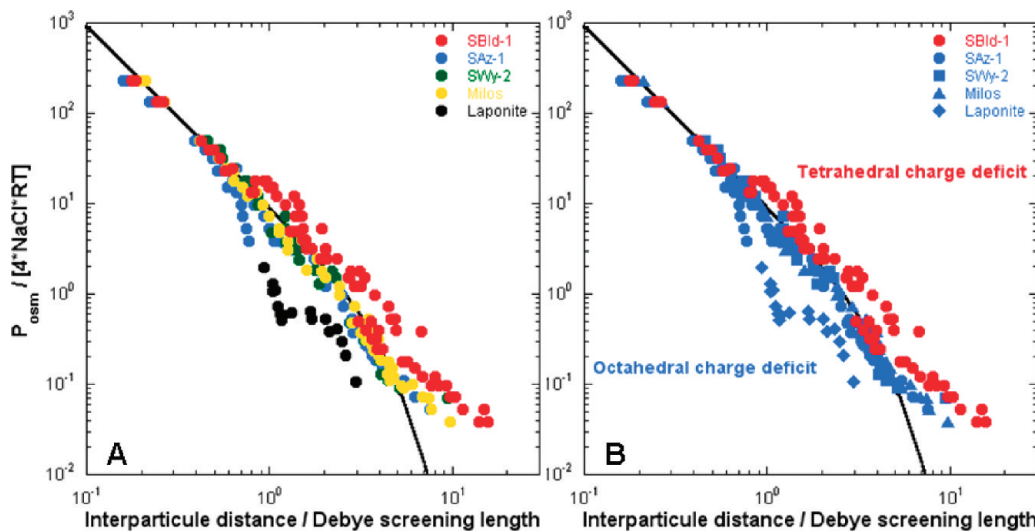


Figure 7. Variation of the reduced osmotic pressure as a function of the experimental interparticle distance with (A) the type of clay and (B) the charge location. The thick black line corresponds to the asymptotic solution calculated from eq A6 in ref 72 with $\sigma = -0.11 \text{ C} \cdot \text{m}^{-2}$ and $H \gg 0.3 \text{ nm}$ in the case of a symmetrical 1:1 electrolyte solution. (See the text.)

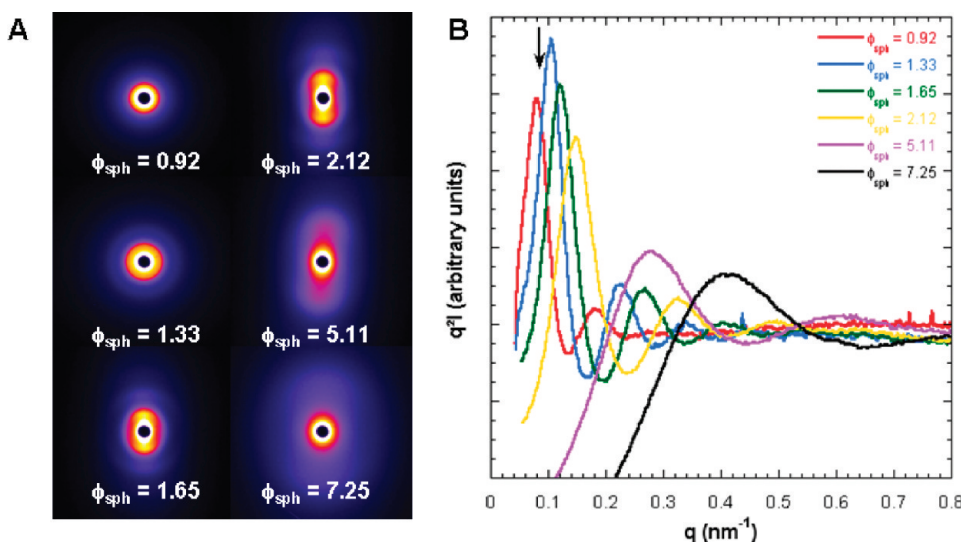


Figure 8. Evolution of the local platelet ordering with increasing spherical volume fraction for size 2 SAZ-1 (ionic strength = 10^{-5} M). (A) 2D SAXS patterns. (B) Variation of the structure factor with q . The black arrow represents the volume fraction at which the sol–gel transition occurs.

local order can be obtained by carefully analyzing the structure factor. In the first step, we focused on Arizona (SAZ-1) montmorillonite suspensions. For such samples, the structural charge is related almost entirely to octahedral substitutions (Table 1). Figure 8 presents the evolution of the structure factor, $q^2 I(q)$, with the clay concentration.

Upon an increase in the spherical volume fraction, the diffuse scattering peaks become obviously stronger until the sol–gel transition is reached. Because the gel state is not at thermodynamic equilibrium,⁵⁴ the particles cannot freely diffuse and reorganize, which may explain the broadening of the correlation peak with increasing volume fraction. Such behavior was also observed with other colloidal suspensions of very different natures.^{89–91} This effect becomes very obvious deep in the gel state.

The ionic strength and average particle size can also affect the local ordering of the platelets. We therefore applied the same

treatment to size 2 Arizona (SAZ-1) suspensions at various ionic strengths (Figure 9) and for different size fractions of Arizona (SAZ-1) suspensions at 10^{-5} M (Figure 10). In both cases, the spherical volume fraction was used to compare samples with identical hydrodynamic volumes.

The effect of ionic strength is rather limited, but the correlation peaks broaden with increasing ionic strength or increasing average particle size, which suggests a disruption of the positional local order. Similar features have been observed for the other clay samples. These results agree with those obtained for nontronites⁷² and show that the smaller the particles, the better their orientation in the suspension.

To gain further insight into the local structure, it is relevant to fit the experimental structure factors. We have recently shown that an approach using the effective Percus–Yevick (PY) model is well suited to reproduce data at thermodynamic equilibrium.⁸⁷

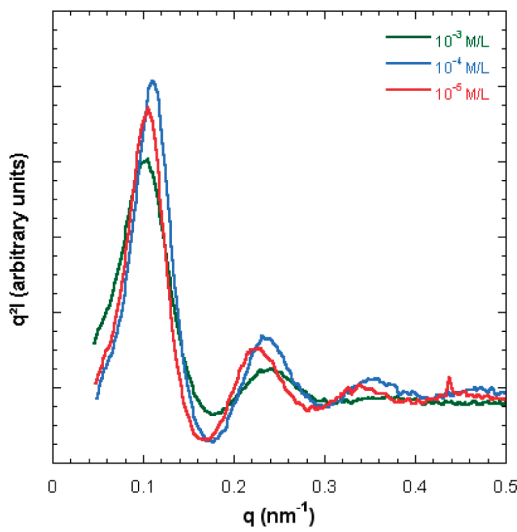


Figure 9. Evolution of the platelet positional local order of size 2 SAz-1 with increasing ionic strength: ionic strength 10^{-5} M, $\phi_{\text{sph}} = 1.52$; ionic strength 10^{-4} M, $\phi_{\text{sph}} = 1.55$; and ionic strength 10^{-3} M, $\phi_{\text{sph}} = 1.51$.

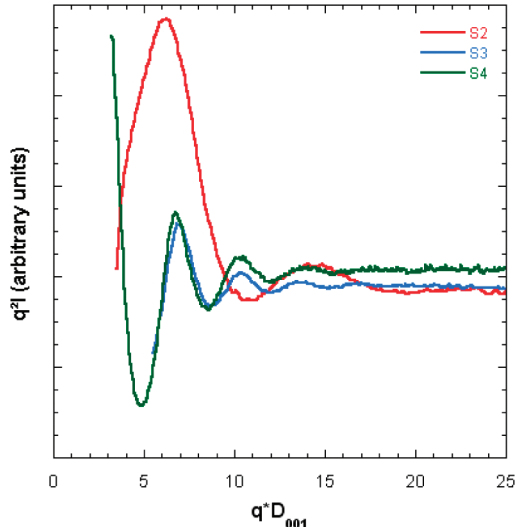


Figure 10. Evolution of the platelet positional local order of SAz-1 at an ionic strength of 10^{-5} M with increasing average size: S2, $\phi_{\text{sph}} = 0.91$; S3, $\phi_{\text{sph}} = 0.89$; and S4, $\phi_{\text{sph}} = 0.86$. The scattering vector modulus q was rescaled by the value of the interparticle distance of the first peak D_{001} .

Because of the strongly anisometric shape of clay particles, the equivalent Percus–Yevick diameter $2a_{\text{PY}}$ corresponds to the average interparticle distance. Therefore, the experimental curves can be fitted by adjusting only the equivalent Percus–Yevick volume fraction ϕ^{PY} . The interparticle contribution to the structure factor can then be obtained by calculating the coexcluded volume occupied by the effective particles (Figure 11).

The sweeping volume corresponding to the volume displaced upon one rotation involving a change in the particle director is described by a sphere encompassing the effective ellipsoid (Figure 11A) as

$$V_{\text{sweep}} = \frac{\pi}{6} \langle D \rangle^3 \quad (6)$$

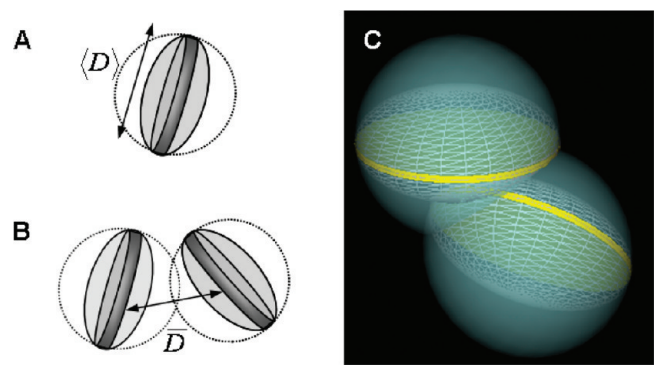


Figure 11. Schematic representation of (A) the sweeping volume V_{sweep} (eq 66) and (B) the intersection volume V_{covolume} between two spheres separated by an average interparticle distance \bar{D} . (C) Spatial representation of the intersection volume.

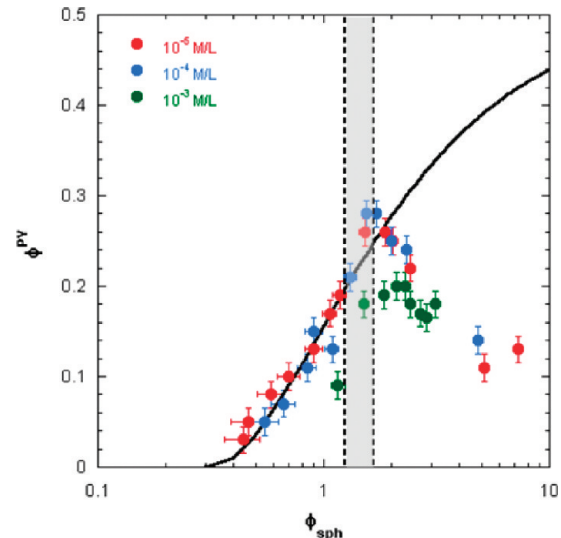


Figure 12. Variation of the Percus–Yevick volume fraction vs the spherical volume fraction for size 2 SAz-1 at various ionic strengths. The solid line corresponds to eq 7. The gray zone corresponds to the sol–gel transition.⁹²

Considering now spheres separated by an average distance \bar{D} , the cosweeping volume per unit sphere can be written as

$$\langle \phi \rangle^{\text{CS}} = \frac{1}{2} \frac{V_{\text{covolume}}}{\pi \langle D \rangle^3} = \frac{1}{4} \left(2 + \frac{\bar{D}}{\langle D \rangle} \right) \left(1 - \frac{\bar{D}}{\langle D \rangle} \right)^2 \quad (7)$$

with V_{covolume} being the intersection volume between two spheres (Figure 11B,C) whose diameter $\langle D \rangle$ is that of the particle. As discussed recently,⁸⁷ the cosweeping volume $\langle \phi \rangle^{\text{CS}}$ can be directly assimilated to the PY volume ϕ^{PY} . Figure 12 presents such a comparison for the case of size 2 SAz-1 as a function of the spherical volume fraction and at different ionic strengths.

An excellent agreement between calculated and experimental data is observed for all samples at low ionic strength and below the gel transition. Deviations are observed deep in the gel and for an ionic strength of 10^{-3} M although all data are located in the range where the PY approximation applies ($\phi^{\text{PY}} < 0.45$). As previously discussed, the discrepancy in the gel region is probably

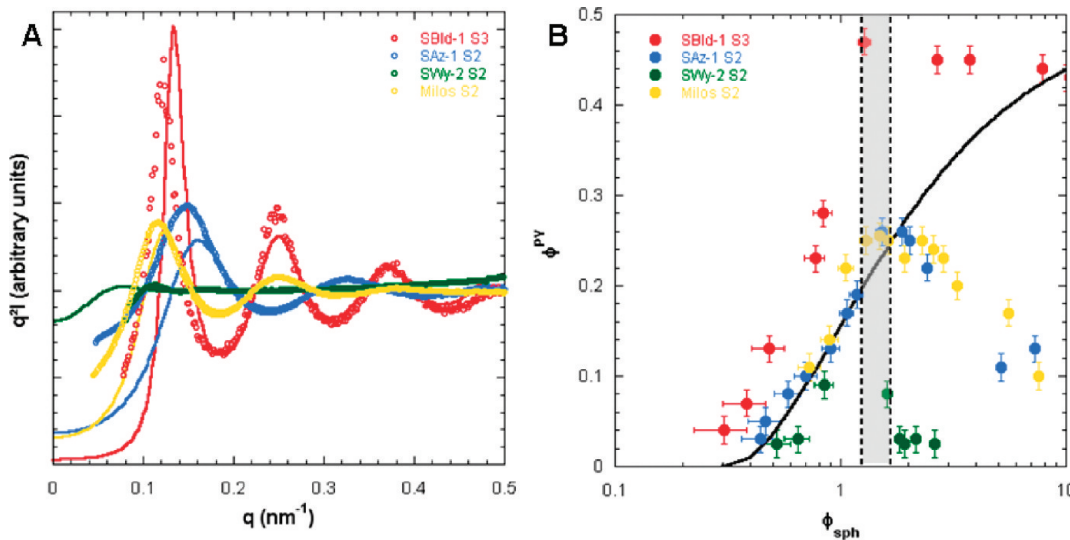


Figure 13. Influence of the clay type at an average size of ~ 200 nm and at an ionic strength of 10^{-5} M. (A) Fits of the structure factors by the effective Percus–Yevick model: red, SBId-1 S3 $\phi_{\text{sph}} = 2.68$; blue, SAz-1 S2 $\phi_{\text{sph}} = 2.43$; green, SWy-2 S2 $\phi_{\text{sph}} = 2.59$; and yellow, Milos S2 $\phi_{\text{sph}} = 2.57$. (B) Evolution of the Percus–Yevick volume fraction with the spherical volume fraction. The solid line corresponds to eq 7. The gray zone corresponds to the sol–gel transition.⁹²

related to the fact that such samples are not at thermodynamic equilibrium. Deviations observed for the highest ionic strength investigated can be assigned to a decrease in ionic repulsions whereas the model can be applied only to truly repulsive interactions. To compare different clay samples, the same treatment was applied to beidellite and montmorillonites at an ionic strength of 10^{-5} M using samples with equivalent diameters. Figure 13A displays the fits of PY structure factors for the four clays at equivalent spherical volume fractions. The theoretical curves were adjusted on the second modulation of the structure factor.

The structure factors are significantly different depending on the type of clay. Beidellite displays sharp peaks indicating a strong ordering of the platelets. This strongly contrasts with the case of Wyoming (SWy-2) montmorillonites, where a weak, broad modulation is observed, which indicates a rather disorganized structure. The behavior of Arizona (SAz-1) and Milos montmorillonites is intermediate because these two samples display clear scattering peaks that are, however, significantly broader than those observed for beidellite. Figure 13B presents the values of ϕ^{PY} obtained from the fits of the structure factors at all of the investigated volume fractions. At low volume fraction, the PY volume fractions are in reasonable agreement with the model. In the gel state and except for beidellite whose PY volume fractions are still higher than 0.4, all samples display data points that are significantly lower than the model, which again suggests that such samples are not at thermodynamic equilibrium. Generally, the PY volume fractions decrease in the sequence SBId-1 > Milos \approx SAz-1 > SWy-2. It must be pointed out that the values for beidellite are always above the model. Even if this feature remains unclear, this could indicate that the repulsive interactions between the beidellite platelets are stronger than for the other types of clay, inducing a better organization of the beidellite particles in suspension. It is striking that the sequence thus obtained from structure factor analysis is roughly the same as that derived from osmotic pressure measurements, which clearly shows that the improvement of the positional liquidlike order of the particles is closely related to the charge location. However, the PB equation

does not allow us to discriminate electrostatic behavior within montmorillonites. Furthermore, Milos and Wyoming (SWy-2) montmorillonites have similar chemical formulas but present strong differences in their structure factors. This feature remains unclear and cannot be explained solely on the basis of electrostatic interactions. Finally, the elucidation of the behavior at low ionic strength of the various clay samples presented in this work should help us to understand their macroscopic mechanical properties (yield stress, elasticity, shear thinning, etc.). This will be investigated in detail in a companion paper.⁹²

ASSOCIATED CONTENT

S Supporting Information. Additional swelling laws. This material is available free of charge via the Internet at <http://pubs.acs.org>.

AUTHOR INFORMATION

Corresponding Author

*E-mail: erwan.paineau@ensg.inpl-nancy.fr; laurent.michot@ensg.inpl-nancy.fr.

ACKNOWLEDGMENT

We gratefully acknowledge the French ANR funding agency for financial support under the ANR-07-BLANC-0194 program. The DESY and ESRF synchrotron facilities are also acknowledged for awarding beam time. We also thank Dr. Jaafar Ghanbaja for TEM micrograph acquisition, Dr. Christian Moyne for Poisson–Boltzmann calculations, Dr. Frederic Pignon and Dr. Céline Martin for providing Laponite data, and Dr. Jérôme F. L. Duval for stimulating discussions.

REFERENCES

- Odom, I. E. *Philos. Trans. R. Soc. London, Ser. A* **1984**, *311*, 391–409.

- (2) Harvey, C. C.; Lagaly, G. In *Handbook of Clay Science*; Bergaya, F., Theng, B. G., Lagaly, G., Eds.; Elsevier: New York, 2006; Chapter 10.1.
- (3) Carretero, M. I. *Appl. Clay Sci.* **2002**, *21*, 155–163.
- (4) Freundlich, H. *Kolloid-Z.* **1928**, *46*, 289–307.
- (5) Langmuir, I. *J. Chem. Phys.* **1938**, *6*, 873–896.
- (6) Bihannic, I.; Michot, L. J.; Lartiges, B. S.; Vantelon, D.; Labille, J.; Thomas, F.; Susini, J.; Salomé, M.; Fayard, B. *Langmuir* **2001**, *17*, 4144–4147.
- (7) Zocher, H. Z. *Anorg. Allg. Chem.* **1925**, *147*, 91–110.
- (8) Davidson, P.; Garreau, A.; Livage, J. *Liq. Cryst.* **1994**, *16*, 905–910.
- (9) Miyamoto, N.; Nakato, T. *Adv. Mater.* **2002**, *14*, 1267–1270.
- (10) Miyamoto, N.; Nakato, T. *J. Phys. Chem. B* **2004**, *108*, 6152–6159.
- (11) Dessimoz, A.; Chiche, D.; Davidson, P.; Panine, P.; Chanéac, C.; Jolivet, J. P. *J. Am. Chem. Soc.* **2007**, *129*, 5904–5909.
- (12) Van der Kooij, F. M.; Lekkerkerker, H. N. W. *J. Phys. Chem. B* **1998**, *102*, 7829–7832.
- (13) Van der Kooij, F. M.; Kassapidou, K.; Lekkerkerker, H. N. W. *Nature* **2001**, *406*, 868–871.
- (14) Van der Kooij, F. M.; Lekkerkerker, H. N. W. *Langmuir* **2004**, *20*, 8582–8586.
- (15) Mourad, M. C. D.; Wijnhoven, J. E. G. J.; Van't Zand, D. D.; Van der Beek, D.; Lekkerkerker, H. N. W. *Philos. Trans. R. Soc. London, Ser. A* **2006**, *364*, 2807–2816.
- (16) Brown, A. B. D.; Clarke, S. M.; Rennie, A. R. *Langmuir* **1998**, *14*, 3129–3132.
- (17) Brown, A. B. D.; Ferrero, C.; Narayanan, T.; Rennie, A. R. *Eur. Phys. J. B* **1999**, *11*, 481–489.
- (18) Buining, P. A.; Lekkerkerker, H. N. W. *J. Phys. Chem.* **1993**, *97*, 11510–11516.
- (19) Van Bruggen, M. P. B.; Van der Kooij, F. M.; Lekkerkerker, H. N. W. *J. Phys.: Condens. Matter* **1996**, *8*, 9451–9456.
- (20) Van Bruggen, M. P. B.; Lekkerkerker, H. N. W. *Langmuir* **2002**, *18*, 7141–7145.
- (21) Lemaire, B. J.; Davidson, P.; Ferré, J.; Jamet, J. P.; Panine, P.; Dozov, I.; Jolivet, J. P. *Phys. Rev. Lett.* **2002**, *88*, 125507.
- (22) Vroege, G. J.; Thies-Weesie, D. M. E.; Petukhov, A. V.; Lemaire, B. J.; Davidson, P. *Adv. Mater.* **2006**, *18*, 2565–2568.
- (23) Liu, S.; Zhang, J.; Wang, N.; Liu, W.; Zhang, C.; Sun, D. *Chem. Mater.* **2003**, *15*, 3240–3241.
- (24) Mourad, M. C. D.; Devid, E. J.; Van Schooneveld, M. M.; Vonk, C.; Lekkerkerker, H. N. W. *J. Phys. Chem. B* **2008**, *112*, 10142–10152.
- (25) Gabriel, J. C. P.; Camerel, F.; Lemaire, B. J.; Desvaux, H.; Davidson, P.; Batail, P. *Nature* **2001**, *413*, 504–508.
- (26) Michot, L. J.; Bihannic, I.; Maddi, S.; Funari, S. S.; Baravian, C.; Levitz, P.; Davidson, P. *Proc. Natl. Acad. Sci. U.S.A.* **2006**, *44*, 16101–16104.
- (27) Mourchid, A.; Delville, A.; Lambard, J.; Lécolier, E.; Levitz, P. *Langmuir* **1995**, *11*, 1942–1950.
- (28) Mourchid, A.; Delville, A.; Levitz, P. *Faraday Discuss.* **1995**, *101*, 275–285.
- (29) Mourchid, A.; Lécolier, E.; Van Damme, H.; Levitz, P. *Langmuir* **1998**, *14*, 4718–4723.
- (30) Gabriel, J. C. P.; Sanchez, C.; Davidson, P. *J. Phys. Chem.* **1996**, *100*, 11139–11143.
- (31) Michot, L. J.; Bihannic, I.; Porsch, K.; Maddi, S.; Baravian, C.; Mougel, J.; Levitz, P. *Langmuir* **2004**, *20*, 10829–10837.
- (32) Bourgton, G.; Squires, L. *J. Phys. Chem.* **1936**, *40*, 1041–1053.
- (33) Van Olphen, H. *Discuss. Faraday Soc.* **1951**, *11*, 82–84.
- (34) Van Olphen, H. *J. Colloid Sci.* **1964**, *19*, 313–322.
- (35) Dijkstra, M.; Hansen, J. P.; Madden, P. A. *Phys. Rev. Lett.* **1995**, *75*, 2236–2239.
- (36) Norrish, K. *Discuss. Faraday Soc.* **1954**, *18*, 120–134.
- (37) Callaghan, I. C.; Ottewill, R. H. *Faraday Discuss.* **1974**, *57*, 110–118.
- (38) Ramsay, J. D. F. *J. Colloid Interface Sci.* **1986**, *109*, 441–447.
- (39) Avery, R. G.; Ramsay, J. D. F. *J. Colloid Interface Sci.* **1986**, *109*, 448–454.
- (40) Abend, S.; Lagaly, G. *Appl. Clay Sci.* **2000**, *16*, 201–227.
- (41) Kroon, M.; Vos, W. L.; Wegdam, G. H. *Int. J. Thermophys.* **1998**, *19*, 887–894.
- (42) Saunders, J. M.; Goodwin, J. W.; Richardson, R. M.; Vincent, B. *J. Phys. Chem. B* **1999**, *103*, 9211–9218.
- (43) Lemaire, B. J.; Panine, P.; Gabriel, J. C. P.; Davidson, P. *Europophys. Lett.* **2002**, *59*, 55–61.
- (44) DiMasi, E.; Fossum, J. O.; Gog, T.; Venkataraman, C. *Phys. Rev. E* **2001**, *64*, 061704.
- (45) Martin, C.; Pignon, F.; Piau, J. M.; Magnin, A.; Lindner, P.; Cabane, B. *Phys. Rev. E* **2002**, *66*, 021401.
- (46) Martin, C.; Pignon, F.; Magnin, A.; Meireles, M.; Lelièvre, V.; Lindner, P.; Cabane, B. *Langmuir* **2006**, *22*, 4065–4075.
- (47) Bhatia, S.; Barker, J.; Mourchid, A. *Langmuir* **2003**, *19*, 532–535.
- (48) Mongondry, P.; Tassin, J. F.; Nicolai, T. *J. Colloid Interface Sci.* **2005**, *283*, 397–405.
- (49) Fonseca, M. D.; Méheust, Y.; Fossum, J. O.; Fnudsen, K. D.; Parmar, K. P. S. *Phys. Rev. E* **2009**, *79*, 021402.
- (50) Kroon, M.; Wegdam, G. H.; Sprik, R. *Phys. Rev. E* **1996**, *54*, 6541–6550.
- (51) Bonn, D.; Tanaka, H.; Wegdam, G.; Kellay, H.; Meunier, J. *Europophys. Lett.* **1998**, *45*, 52–57.
- (52) Levitz, P.; Lécolier, E.; Mourchid, A.; Delville, A.; Lyonnard, S. *Europophys. Lett.* **2000**, *49*, 672–677.
- (53) Knaebel, A.; Bellour, M.; Munch, J. P.; Viasnoff, V.; Lequeux, F.; Harden, J. L. *Europophys. Lett.* **2000**, *52*, 73–79.
- (54) Tanaka, H.; Meunier, J.; Bonn, D. *Phys. Rev. E* **2004**, *69*, 031404.
- (55) Tanaka, H.; Jabbari-Farouil, S.; Meunier, J.; Bonn, D. *Phys. Rev. E* **2005**, *71*, 021402.
- (56) Ianni, F.; Di Leonardo, R.; Gentilini, S.; Ruocco, G. *Phys. Rev. E* **2007**, *75*, 011408.
- (57) Ruzicka, B.; Zulian, L.; Ruocco, G. *J. Phys.: Condens. Matter* **2004**, *16*, S4993–S5002.
- (58) Ruzicka, B.; Zulian, L.; Zaccarelli, E.; Angelini, R.; Sztucki, M.; Moussaid, A.; Ruocco, G. *Phys. Rev. Lett.* **2010**, *104*, 085701.
- (59) Ramsay, J. D. F.; Swanton, S. W.; Bunce, J. *J. Chem. Soc., Faraday Trans. 1990*, *86*, 3919–3926.
- (60) Ramsay, J. D. F.; Lindner, P. *J. Chem. Soc., Faraday Trans. 1993*, *89*, 4207–4214.
- (61) Baravian, C.; Vantelon, D.; Thomas, F. *Langmuir* **2003**, *19*, 8109–8114.
- (62) Ten Brinke, A. J. W.; Bailey, L.; Lekkerkerker, H. N. W.; Maitland, G. C. *Soft Matter* **2007**, *3*, 1145–1162.
- (63) Duval, F. P.; Porion, P.; Faugère, A. M.; Van Damme, H. *J. Colloid Interface Sci.* **2001**, *242*, 319–326.
- (64) Porion, P.; Al-Mukhtar, M.; Faugère, A. M.; Delville, A. *J. Phys. Chem. B* **2004**, *108*, 10825–10831.
- (65) Spitzer, J. J. *Langmuir* **1989**, *5*, 199–205.
- (66) Delville, A.; Laszlo, P. *Langmuir* **1990**, *6*, 1289–1294.
- (67) Delville, A. *Langmuir* **1994**, *10*, 395–402.
- (68) Agra, R.; Trizac, E.; Bocquet, L. *Eur. Phys. J. E* **2004**, *15*, 345–357.
- (69) Jönsson, B.; Labbez, C.; Cabane, B. *Langmuir* **2008**, *24*, 11406–11413.
- (70) Lubertkin, S. D.; Middleton, S. R.; Ottewill, R. H. *Philos. Trans. R. Soc. London, Ser. A* **1984**, *311*, 353–368.
- (71) Michot, L. J.; Bihannic, I.; Maddi, S.; Baravian, C.; Levitz, P.; Davidson, P. *Langmuir* **2008**, *24*, 3127–3139.
- (72) Michot, L. J.; Baravian, C.; Bihannic, I.; Maddi, S.; Moyne, C.; Duval, J. F. L.; Levitz, P.; Davidson, P. *Langmuir* **2009**, *25*, 127–139.
- (73) Michot, L. J.; Paineau, E.; Bihannic, I.; Maddi, S.; Duval, J. F. L.; Baravian, C.; Davidson, P.; Levitz, P. *Clay Miner.*, in press.
- (74) Paineau, E.; Antonova, K.; Baravian, C.; Bihannic, I.; Davidson, P.; Dozov, I.; Impérator-Clerc, M.; Levitz, P.; Madsen, A.; Meneau, F.; Michot, L. J. *J. Phys. Chem. B* **2009**, *113*, 15858–15869.
- (75) (a) It must be pointed out that recent work (see the following references) has shown a gravity-induced isotropic/nematic transition in high-charge synthetic fluorohectorite, an octahedrally substituted clay mineral. However, the transition involves stacks of platelets rather than individual layers, and the situation is then different from the one analyzed in the present paper. (b) Hemmen, H.; Ringdal, N. I.; De Azevedo, E. N.; Engelsberg, M.; Hansen, E. L.; Méheust, Y.; Fossum, J. O.; Knudsen, K. D.

Langmuir **2009**, *25*, 12507–12515. (c) Miyamoto, N.; Iijima, H.; Ohkubo, H.; Yamauchi, Y. *Chem. Commun.* **2010**, *46*, 4166–4168.

(76) Ross, C. S.; Hendricks, S. B. *U.S. Geol. Surv. Prof. Pap.* **1945**, *205B*, 23–79.

(77) Güven, N. In *Hydrous Phyllosilicates: (Exclusive of Micas)*; Bailey, S. W., Ed.; Mineralogical Society of America: Washington, DC, 1988; Vol. 19, Chapter 13, pp 497–559.

(78) Vantelon, D.; Montargès-Pelletier, E.; Michot, L. J.; Briois, V.; Pelletier, M.; Thomas, F. *Phys. Chem. Miner.* **2003**, *30*, 44–53.

(79) Orsini, L.; Remy, J. C.; Henon, P. *Sci. Sol.* **1976**, *4*, 269–275.

(80) Parsegian, V. A.; Rand, R. P.; Fuller, N. L.; Rau, D. C. *Methods Enzymol.* **1986**, *127*, 400–416.

(81) Michot, L. J.; Bihannic, I.; Pelletier, M.; Rinnert, E.; Robert, J. L. *Am. Mineral.* **2005**, *90*, 166–172.

(82) Bérend, I.; Cases, J. M.; François, M.; Uriot, J. P.; Michot, L. J.; Masion, A.; Thomas, F. *Clays Clay Miner.* **1995**, *43*, 324–336.

(83) Güven, N.; Pease, R. W. *Clays Clay Miner.* **1975**, *23*, 187–191.

(84) Cadene, A.; Durand-Vidal, S.; Turq, P.; Brendle, J. J. *Colloid Interface Sci.* **2005**, *285*, 719–730.

(85) Mourad, M. C. D.; Byelov, D.; Petukhov, A. V.; Matthijs de Winter, D. A.; Verkleij, A. J.; Lekkerkerker, H. N. W. *J. Phys. Chem. B* **2009**, *113*, 11604–11613.

(86) Vantelon, D.; Belkhou, R.; Bihannic, I.; Michot, L. J.; Montargès-Pelletier, E.; Robert, J. L. *Phys. Chem. Miner.* **2009**, *36*, 593–602.

(87) Baravian, C.; Michot, L. J.; Paineau, E.; Bihannic, I.; Davidson, P.; Impérator-Clerc, M.; Belamie, E.; Levitz, P. *Europhys. Lett.* **2010**, *90*, 36005.

(88) Because of the Gauss theorem, the electrostatic potential should not depend on its location.

(89) Pelletier, O.; Davidson, P.; Bourgaux, C.; Livage, J. *Europhys. Lett.* **1999**, *48*, 53–59.

(90) Belamie, E.; Davidson, P.; Giraud-Guille, M. M. *J. Phys. Chem. B* **2004**, *108*, 14991–15000.

(91) Gobeaux, F.; Belamie, E.; Mosser, G.; Davidson, P.; Panine, P.; Giraud-Guille, M. M. *Langmuir* **2007**, *23*, 6411–6417.

(92) Paineau, E.; Michot, L. J.; Bihannic, I.; Baravian, C. *Langmuir*, submitted for publication.